Metallophysics and Advanced Technologies
Металофіз. новітні технол.
Metallofiz. Noveishie Tekhnol.
2020, vol. 42, No. 8, pp. 1065–1078
https://doi.org/10.15407/mfint.42.08.1065
Reprints available directly from the publisher

AMORPHOUS AND LIQUID STATES

PACS numbers: 61.05.cp, 61.43.Dq, 61.72.Cc, 64.70.kd, 68.37.Lp, 68.55.A-

'*In-Situ*' Electron Microscopy Video Registration of Thin Amorphous Films Crystallization

A. G. Bagmut

National Technical University 'Kharkiv Polytechnic Institute',
2 Kyrpychov Str.,
UA-61002 Kharkiv, Ukraine

The article summarizes the results of electron microscopic studies of '*in situ*' crystallization of thin amorphous films. Data analysis is carried out based on the classification scheme of electron-beam crystallization of films, including structural-morphological and numerical characteristics. Layer polymorphous crystallization (as the analogue of Frank–van der Merwe growth mode), island polymorphous crystallization (as an analogue of the Volmer–Weber growth mode) and dendrite polymorphous crystallization (as an analogue of the Stransky–Krastanov growth mode) are identified. For each type of crystallization a dimensionless parameter of the relative length δ_0 is determined. It is equal to the ratio of the characteristic length to the value, related to the size of the unit cell of the crystal. Based on the electron microscopic video registration of the process, kinetic crystallization curves are built for each type of the transformation.

Key words: crystallization kinetics, crystal growth modes, TEM, amorphous films, relative length, video registration.

У статті узагальнено результати електронно-мікроскопічних досліджень «*in situ*» кристалізації тонких аморфних плівок. Аналіз даних проведено за допомогою класифікаційної схеми електронно-променевої кристалізації аморфних плівок, що містить структурно-морфологічні і числові характеристики. Виділено шарову поліморфну кристалізацію (як аналог моди росту Франка–ван-дер-Мерве), острівцеву поліморфну кристалізацію (як аналог моди росту Фольмера–Вебера) і дендритну поліморфну кристалізацію (як аналог моди росту Странського–Крастанова). Для ко-

Corresponding author: Aleksandr Grigor'evich Bagmut
E-mail: agbagmut@gmail.com

Citation: A. G. Bagmut, '*In-Situ*' Electron Microscopy Video Registration of Thin Amorphous Films Crystallization, *Metallofiz. Noveishie Tekhnol.*, **42**, No. 8: 1065–1078 (2020), DOI: 10.15407/mfint.42.08.1065.

жного типу кристалізації визначено безрозмірний параметр відносної довжини δ_0, що дорівнює відношенню характеристичної довжини до величини, пов'язаної з розміром елементарної комірки кристала. На основі електронно-мікроскопічної відеореєстрації процесу для кожного типу перетворень побудовано кінетичні криві кристалізації.

Ключові слова: кінетика кристалізації, моди росту кристалів, ПЕМ, аморфні плівки, відносна довжина, відеореєстрація.

(Received December 5, 2019; in final version, April 15, 2020)

1. INTRODUCTION

Amorphous materials in the film state are widely used in various branches of technology. The stable operation of electronic devices based on amorphous matter implies, in some cases, the invariance of the amorphous structure (for example, photo electronic converters). In some cases, the effective operation of the device is associated with the possibility of multiple phase transformations of noncrystalline state–crystal–noncrystalline state type (for example, optical recording media) occurring at the local site of an object. In all the cases, knowledge of the features of the transition of amorphous substance to crystalline substance and the systematization of crystallization reactions according to the selected features are necessary.

Amorphous films can crystallize spontaneously or under the influence of the physical action, *i.e.* to pass from a metastable noncrystalline solid state to a stable crystalline state. In general, crystallization occurs according to one of the following schemes [1]:

1. Polymorphous crystallization. This is the simplest type of transformation in which the amorphous substance transforms into the crystalline one without changing of the composition. This is the characteristic of both pure elements and stoichiometric chemical compounds.

2. The predominant crystallization of one of the phases on the first stage of the process and the subsequent crystallization of the matrix on the second stage.

3. Eutectic crystallization, in which two crystalline phases segregate almost simultaneously. The implementation of the type of crystallization reaction is predetermined by the type of dependence of the free energy of various phases on the concentration of chemical elements. The rate (speed) of the transformation is determined by both the crystal growth rate and the rate of formation of crystallization centres. Depending on the type of the process that prevails, the division is made into the crystallization controlled by growth and the crystallization controlled by nucleation of crystals [2].

Numerous '*in situ*' electron microscopy studies have proved that polymorphic crystallization of thin amorphous films can be adequately

described by phenomenological scheme that includes the following types (modes) of crystal growth in the amorphous matrix [3–5].

1. Layer polymorphous crystallization (LPC), which is considered as the analogy of layer-by-layer film growth upon condensation of vapour on a substrate (Frank–van der Merwe (FM) growth mode). Similarly with the Bauer criterion [6, 7], the LPC is realized when the inequality $\sigma_a \geq \sigma_c + \sigma_{ac} + \varepsilon_d$ takes place. Here σ_a, σ_c and σ_{ac} are the surface energy of the amorphous phase–vacuum interface, the crystalline phase–vacuum interface, and the surface energy amorphous–crystalline phase, respectively. ε_d is the strain energy of the growing crystalline layer.

2. Island polymorphous crystallization (IPC), which is the analogy of Volmer–Weber (VW) growth mode (island growth during vapour condensation on a substrate). IPC is realized when the opposite inequality $\sigma_a \leq \sigma_c + \sigma_{ac} + \varepsilon_d$ is satisfied.

3. Dendrite polymorphous crystallization (DPC), which can be compared with Stransky–Krastanov (SK) growth mode (single-crystal layer and the subsequent growth of islands on it). DPC is realized when the inequality $\sigma_a \geq \sigma_c + \sigma_{ac} + \varepsilon_d$ is initially satisfied (a single crystal grows in the form of a the first-order dendrite branch), and after reaching the critical size of the crystal, islands grow on its lateral surface (the inequality $\sigma_a \leq \sigma_c + \sigma_{ac} + \varepsilon_d$), which form a polycrystalline interlayer. Dendrite branches of the second and higher order are formed in the process of geometric selection of grains growing from this layer. Table 1 compares the phase transformations of the amorphous phase–the crystal (upon electron beam crystallization of the amorphous film) and the vapour–crystal (upon vapour deposition on the substrate).

Observation and video registration of the processes of structure formation directly in the column of the electron microscope (so-called '*in situ*' technique) are an efficient method for studying crystal growth upon vapour condensation on a substrate [8]. The results of studies us-

TABLE 1. Comparison of phase transformations 'amorphous phase–crystal' and 'vapour–crystal'.

Amorphous phase–crystal			Vapour–crystal	
Type of crystallization	Requirement	Relative length δ_0	Growth mode	Requirement
LPC	$\sigma_a \geq \sigma_c + \sigma_{ac} + \varepsilon_d$	2500–4700	FM	$\gamma_s \geq \gamma_f + \gamma_{sf}$
IPC	$\sigma_a \leq \sigma_c + \sigma_{ac} + \varepsilon_d$	100–900	VW	$\gamma_s \leq \gamma_f + \gamma_{sf}$
DPC	Initially $\sigma_a \geq \sigma_c + \sigma_{ac} + \varepsilon_d$, then $\sigma_a \leq \sigma_c + \sigma_{ac} + \varepsilon_d$	~3900	SK	Initially $\gamma_s \geq \gamma_f + \gamma_{sf}$, then $\gamma_s \leq \gamma_f + \gamma_{sf}$

ing video recording '*in situ*' crystal growth in amorphous films are currently very small and incomplete. The purpose of this work is the electron microscope study with '*in situ*' video registration of crystal growth in amorphous films and the systematization of crystallization reactions according to structural and morphological features.

2. EXPERIMENTAL METHOD

Amorphous films are obtained on KCl substrates at room temperature by thermal evaporation of substance in vacuum, by pulsed laser sputtering targets in oxygen atmosphere and by ion-plasma deposition of metal in argon-oxygen mixture. After deposition and after depressurization of the chamber, the films are separated from the substrates in distilled water and transferred onto subject grids for electron microscopic studies. Structural analysis is performed by methods of electron diffraction and transmission electron microscopy, using electron microscopes EM-100L and PEM-100-01 operating at the accelerating voltage of 100 kV. The film thickness ranged from 25 to 30 nm. The phase transformation is initiated by irradiating of the film with the electron beam in the microscope column with the beam current of ~20 μA. The crystallization rate is set by changing the electron current density through the sample, which is 1.1–6.5 $A \cdot mm^{-2}$, depending on the beam focusing. The process of crystallization of the film is recorded from the screen of the electron microscope with Canon Power Shot G15 camera in the video recording mode with the frame rate of 30 s^{-1} [5].

Determination of the crystallization type is made on the value of the relative length δ_0, defined as

$$\delta_0 = D_0/a_0 \tag{1}$$

in the case of LPC, and as

$$\delta_0 = \frac{D_0}{\sqrt[3]{\Omega}} \tag{2}$$

in the case of IPC.

The characteristic unit of length D_0 is the crystal size at time t_0, after which the volume of the amorphous phase decreases by $e = 2.718$; a_0 in the expression (1) is the cell parameter of the growing crystal; Ω in the expression (2) represents the volume of elementary cell of the growing crystal. The difference in the definition of δ_0 is explained by the fact, that in the case with LPC a single crystal is formed in the investigated area (with a_0 cell parameter), and in the case with IPC—polycrystalline film with disoriented grains.

3. RESULTS AND DISCUSSIONS

3.1. Layer Polymorphous Crystallization as the Morphological Analogue of the Frank–van der Merwe growth Mode

LPC mode is mostly typical for amorphous films of semiconductors (Se, Te, Sb, Sb_2S_3, Sb_2Se_3, *etc.*) and oxides (ReO_3, Cr_2O_3, V_2O_3, Fe_2O_3, Nb_2O_5, *etc.*) [8]. As the result of thermal (or radiation) exposure in thin surface layer of the amorphous film, a crystal is formed which is growing is such a way, that its growth rate in the tangential direction (υ_τ) significantly exceeds its growth rate in the normal direction to the film surface (υ_n). The crystalline layer 'spreads' over the surface of the amorphous film. As in the case of the FM growth mode of the crystalline layer upon vapour condensation on the substrate, the LPC mode assumes the presence of steps and layers moving at different speeds parallel to the film surface [10]. Figure 1 illustrates the motion of the two-layer crystallization front in the amorphous Cr_2O_3 film. Initially, the S_1 layer moves with a speed $\upsilon_{1\tau} \approx 0.06$ μm·s^{-1}, and S_2 layer with the lower speed $\upsilon_{2\tau} \approx 0.03$ μm·s^{-1}. Two seconds later this layers merge (Fig. 1, *c*), after that a single crystallization front S_{12} is formed.

During electron beam crystallization of amorphous films under the conception of the LPC mode, the major morphological forms are disk-shaped, sickle-shaped and needle-shaped crystals [8, 11, 12]. Disk-shaped crystals grow with the constant speed υ_τ and with a constant morphology. Figures 2, *a*–*c* show the video registration pictures of the disk-shaped crystal, growing in amorphous film of V_2O_3 disk-shaped crystal. The tangential crystal growth rate υ_τ (defined as the time derivative of the diameter D'_t) is 0.235 μm·s^{-1}. A quadratic dependence of the fraction of the crystallized space x on time t is performed, since the experimental points fit satisfactorily on the curve $x(t) = 0.006t^2 + 0.022$ (Fig. 2, *d*). The dependence of the diameter of the disk-shaped

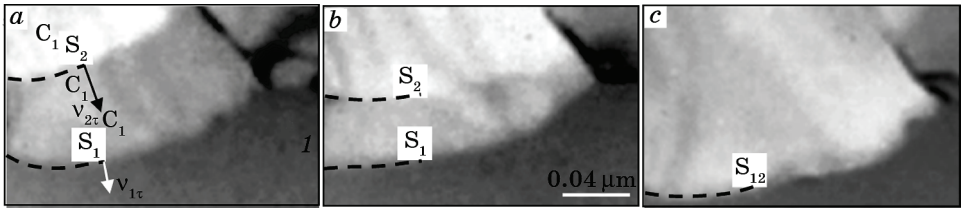

Fig. 1. Film shots of layer crystallization of amorphous film of Cr_2O_3. Photomicrographs correspond to the periods of time t, that passed after the video registration had started: $t = 0$ s (*a*), $t = 0.83$ s (*b*), $t = 1.67$ s (*c*), *1*—amorphous phase, S_1 is the crystallization front, moving with the velocity $\upsilon_{1\tau}$. S_2 is the crystallization front, moving with the velocity $\upsilon_{2\tau}$, S_{12}—crystallization front after the merger of S_1 and S_2.

crystal on x is parabolic: $D(x) = 2.95x^{0.5}$ (Fig. 2, *e*).

The characteristic time t_0 (after which the fraction of the crystalline phases $x = 1 - e^{-1} = 0.632$) is 10.08 s. In this case, the characteristic length is $D_0 = v_\tau t_0 = 2.37$ μm. For V_2O_3 crystal with [001] zone axis, the projection of the unit cell onto the film plane is a rhombus with the side $a_0 = 0.492$ nm and an angle at the apex of 120°. In this case, according to (1), the relative length is $\delta_0 \approx 4817$. It is comparable with $\delta_0 \approx 3200$ for LPC mode of amorphous Cr_2O_3 films, obtained by laser evaporation [5].

In a number of research works, the analogy is noted between the geometric method of constructing the front of the light wave (Huygens principle) and the crystallization front of amorphous film [13–15]. The experimental observation of the envelope of an obstacle (in the form of a hole in the film) by the crystallization front and the subsequent formation of a single crystal layer behind this hole in the same orientation

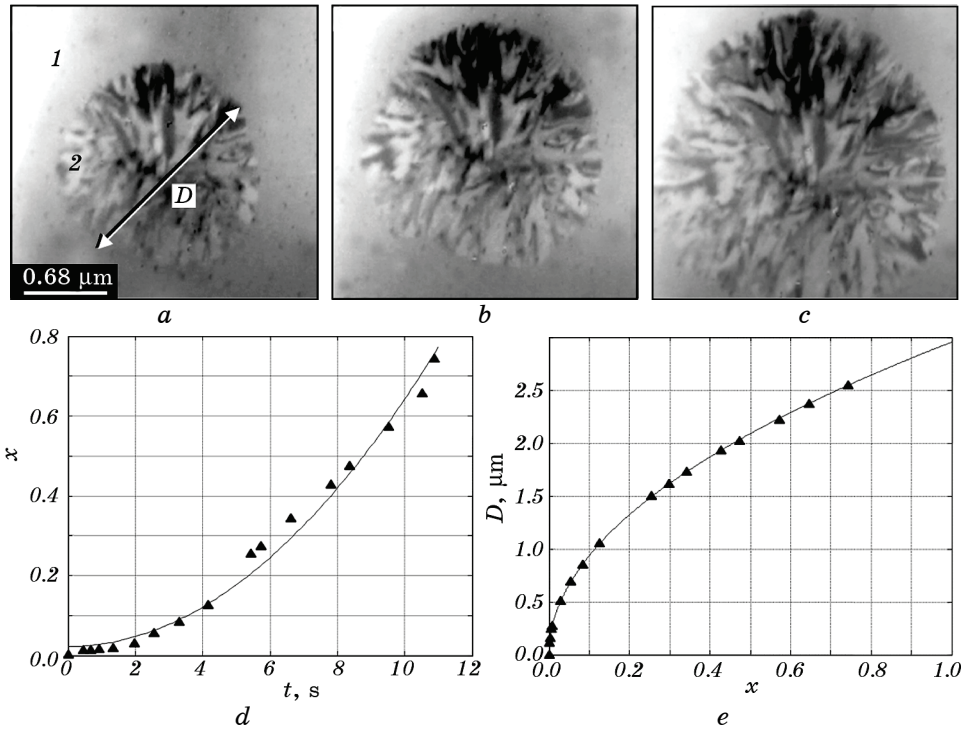

Fig. 2. Layer polymorphous crystallization of amorphous film of V_2O_3. Micrographs of the growth of the disk-shaped crystal (with the speed of $v_\tau = 0.235$ μm·s^{-1}) correspond to the periods of time *t*, that passed after the video registration had started: $t = 0$ s (*a*), $t = 1.43$ s (*b*), $t = 3.19$ s (*c*). Microscopic photographs correspond to kinetic crystallization curves, describing the dependence of the fraction of the crystalline phase $x(t)$ (*d*) and the dependence of the crystal diameter $D(x)$ (*e*), *1*—amorphous phase, *2*—V_2O_3 disk-shaped crystal.

as before the hole, is a confirmation of the above analogy. The single crystallinity of the layer is ensured by the same orientation ('coherence') of the secondary crystallization centres. By virtue of the noted analogy, the term 'coherent' crystallization is applicable to the crystallization of thin films by the LPC mode. The video registration pictures in Fig. 3 illustrate a similar situation. In amorphous film of Cr_2O_3 (space *1*) a disk-shaped crystal (crystal *2*) is growing. In its path there is an obstacle in the form of a needle-shaped Cr_2O_3 crystal (crystal *3*). Figure 3, *c* illustrates the by-pass of the obstacle with the crystallization front, that is similar to the diffraction phenomenon in optics (penetration of the light into the area of geometric shadow).

3.2. Island Polymorphous Crystallization as the Morphological Analogue of the Volmer–Weber Growth Mode

When the secondary crystallization centres are misoriented ('incoherent'), island polymorphic crystallization is realized, which is the analogy of island film growth on a substrate from the vapour phase according to the Volmer–Weber mechanism. For IPC mode the term 'noncoherent' crystallization is applicable. In this case as the result of phase transformation a polycrystalline film is formed. The crystalline phase does not reduce the free surface of the film ('not wetting' condition). This type of crystallization mode is inherent for some amorphous metals and oxides (Ni, Re, Al_2O_3, ZrO_2, *etc.*) [4].

Figure 4, *a* shows the selected area electron diffraction (SAED) pattern of the amorphous film, obtained by electron beam evaporation in vacuum of a YbS sample. The SAED pattern of the film after its partial crystallization and the corresponding electron-microscopic image are shown in Fig. 4, *b* and *c*, respectively. The result of decoding the SAED pattern after crystallization of the film (Fig. 4, *b*) is summarized in Table 2. The interplanar distances *d*, calculated from the measured ring diameters, are compared with the literary works data contained in the tables of the International Center for Diffraction Data—JCPDC. A

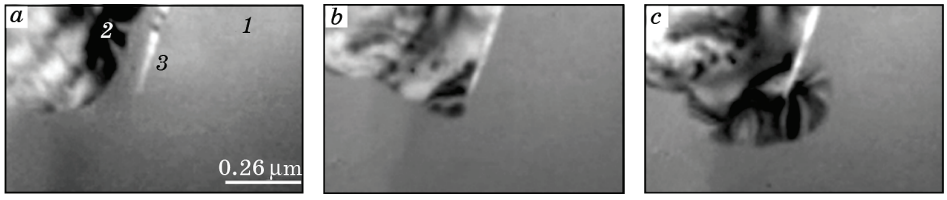

Fig. 3. Bypassing the obstacle by the crystallization front. Photomicrographs correspond to the periods of time *t*, that passed after the video registration had started: $t = 0$ s (*a*), $t = 0.42$ s (*b*), $t = 1.40$ s (*c*), *1*—amorphous phase, *2*—disc-shaped crystal Cr_2O_3, *3*—needle-shaped crystal Cr_2O_3.

TABLE 2. The results of the decoding of the selected area electron diffraction pattern, shown in Fig. 5, *b*.

Ring number	Data of this work			JCPDC table data		
	Interplanar distance, nm	Miller indices	Phase	Interplanar distance, nm	Miller indices	Phase
1	0.643	001		0.650	001	
2	0.323	002		0.324	002	
3	0.289	101		0.2887	101	
4	0.228	102	Yb_2O_2S	0.2287	102	Yb_2O_2S
5	0.186	110		0.1861	110	
6	0.164	200		0.1613	200	
7	0.146	105		0.1450	105	

satisfactory agreement between the experimental data and the data in the tables took place only for Yb_2O_2S (ytterbium oxide sulphide) hexagonal modification with the unit cell parameters $a = 0.3722$ nm and $c = 0.6496$ nm (JCPDS file 26-0614).

Figure 5 illustrates the kinetics of the IPC of amorphous Yb_2O_2S film. Electron microphotographs correspond to the moments of time t, that have passed from the beginning of the recording crystallization process: $t = 1.40$ s (*a*), $t = 2.03$ s (*b*), $t = 2.80$ s (*c*). The average tangential growth rate of crystals $\langle v_\tau \rangle$ (defined as the derivative on time of the average crystal diameter $\langle D \rangle'_t$) is 0.297 μm·s^{-1}. A linear dependence of the density of crystallization centres on time $N(t)$ is fulfilled, since the experimental points fit satisfactorily on the straight line $N(t) = (3.93 \cdot 10^8 t + 9.54 \cdot 10^7)$ cm^{-2} (Fig. 5, *d*). The straight line is constructed according to the measurement of N using the least squares method. The nucleation rate N'_t (the tangent of the angle of inclination

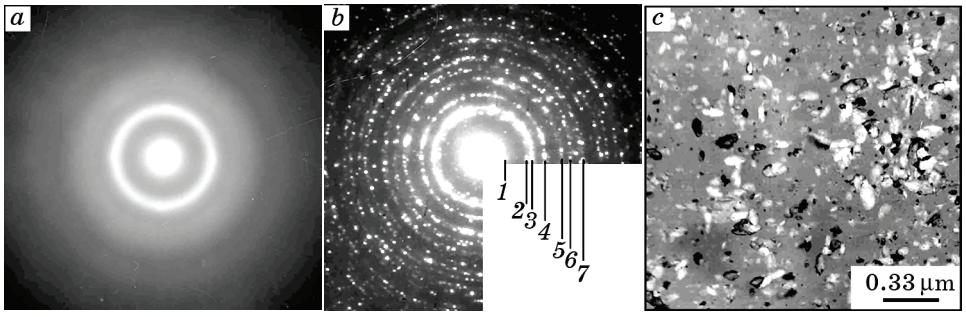

Fig. 4. Electron-beam crystallization of the amorphous Yb_2O_2S film: selected area electron diffraction pattern of the initial state (*a*) and after partial crystallization of the film (*b*); electron microscopic image of the film after partial crystallization (*c*).

of the line to the abscissa axis) is constant and is equal to $3.93 \cdot 10^8$ cm$^{-2} \cdot$s^{-1}.

Figure 5, *e* shows the dependence of the fraction of the crystallized area $x(t)$ in coordinates $\ln[-\ln(1-x)]-\ln t$. The straight line is plotted from the experimental values of x using the least squares method. The correlation coefficient characterizing the tightness of the linear relationship between $\ln[-\ln(1-x)]$ and $\ln t$ is close to unity. The fact that the kinetics of crystallization of the amorphous phase of Yb_2O_2S in these coordinates is described by a straight line indicates the applicability to the process of phase transformation of Johnson–Mail–Avrami–Kolmogorov (JMAK) formula [16]:

$$x = 1 - \exp(-nt^k), \tag{3}$$

where k and n are the kinetic parameters of crystallization. To determine them, expression (3) is written in the form

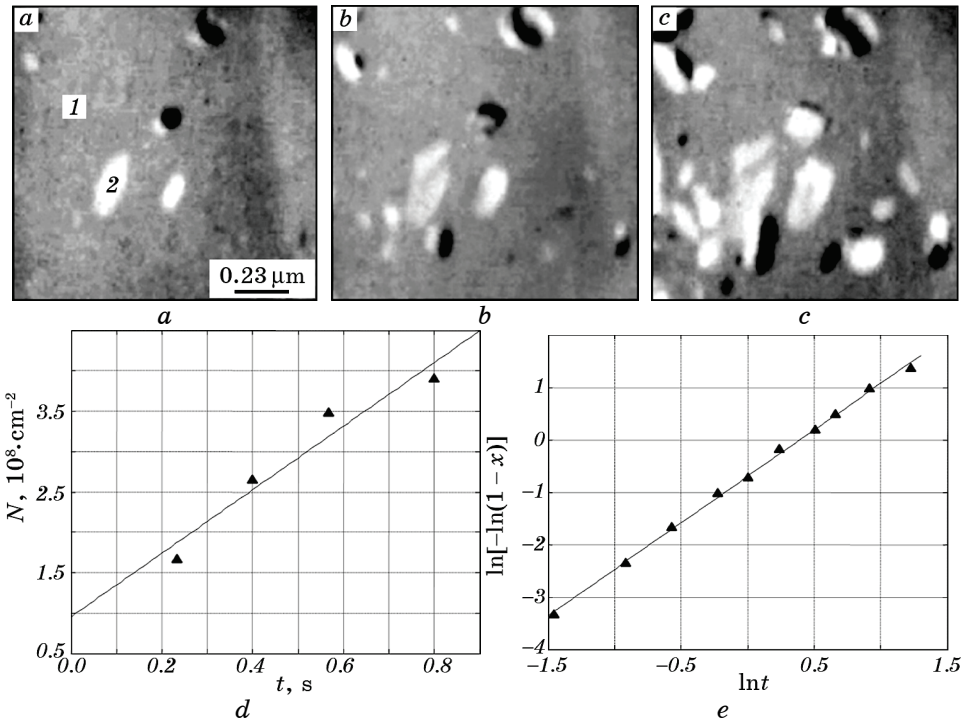

Fig. 5. The kinetics of Yb_2O_2S crystals growth in the amorphous film. The photomicrographs correspond to the periods of time t that passed after the video registration had started: $t = 1.40$ s (*a*), $t = 2.03$ s (*b*), $t = 2.80$ s (*c*). The dependence on time of the crystallization centres $N(t)$ density (*d*) and of the fraction of the crystalline phase $x(t)$ (*e*), *1*—amorphous phase, *2*—Yb_2O_2S crystal.

$$\ln[-\ln(1-x)] = k\ln t + \ln n. \quad (4)$$

According to (4), the coefficient k is the slope of the line to the abscissa, and $\ln n$ is the intersection point of the line with the ordinate (Fig. 5, *e*). In this case, the kinetic parameters of crystallization are as follows: $k = 1.8$ and $n = 0.5s^{-k}$. According to (3), the characteristic unit of time $t_0 = 1.47$ s and the characteristic unit of length $D_0 = t_0\langle v_\tau\rangle$. The volume of unit cell of Yb_2O_2S $\Omega = 7.793\cdot10^{-11}$ μm^3. In this case, according to (2), the relative length $\delta_0 \approx 1030$. It is comparable with the value $\delta_0 \sim 904$ for the special case of the IPC of amorphous ZrO_2 films, deposited by laser evaporation of zirconium in the oxygen atmosphere [9]. The smaller the grain size of the crystallized film, the smaller the dimensionless parameter δ_0. Amorphous films of ZrO_2, deposited by ion-plasma evaporation of Zr in an argon-oxygen atmosphere, during crystallization formed finely crystalline regions with $\delta_0 \sim 118$ [9].

3.3. Dendrite Polymorphous Crystallization as the Morphological Analogue of the Stransky–Krastanov Growth Mode

The impact of the electron beam on amorphous HfO_2 film initiates the amorphous phase—crystal transformation, which is accompanied with the formation of rhombic and monoclinic modifications of HfO_2 crystals [12, 17]. At the final stage of crystallization, the dominant component is the monoclinic modification represented by dendrite HfO_2 crystals. Dendrites are formed from HfO_2 nuclei of both monoclinic and rhombic modifications. In the second case, the size-phase effect takes place. The rhombic modification HfO_2 crystal, having reached the critical size (0.15–0.21 μm), undergoes structural transformation, which is apparently of martensitic nature. The low-temperature monoclinic modification of HfO_2 is formed in the form of plates or needles in the rhombic matrix of HfO_2 as the result of shear diffusionless phase transformation [17].

Figure 6 illustrates the film frames of the dendrites growth in HfO_2 amorphous film. The frames of the micro-film, presented in Fig. 6, *a*, *b*, correspond to one-stage transformation of the amorphous phase—the monoclinic modification of HfO_2. There is linear dependence of the diameter of dendrite D on time t, which indicates its growth with a constant velocity $v_\tau \approx 0.084$ μm·s^{-1} (line *1* in Fig. 7, *a*). The dendrite growth corresponds to the quadratic dependence of the fraction of the crystallized region $x(t) \approx 0.002t^2$ (parabola *1* in Fig. 7, *b*).

The frames in Figures 6, *d*, *e* present the two-stage transformation, which corresponds to the amorphous phase—orthorhombic modification of HfO_2–monoclinic modification of HfO_2. The moment of the structural transformation of the crystal from the orthorhombic to monoclinic modification of HfO_2 corresponds to the film frame, shown

in Fig. 6, *d*.

Crystal of HfO_2, that has reached the critical size of D^*, splits into blocks. The kinks on the dependences $D(t)$ and $x(t)$ correspond to this time. The growth rate increases from $0.057\ \mu m \cdot s^{-1}$ to $0.244\ \mu m \cdot s^{-1}$ (lines *2* and *3* in Fig. 7, *a*). The quadratic dependence $x(t) \approx 0.006t^2$ before the structural transformation (parabola *2* in Fig. 7, *b*) passes into the quadratic dependence $x(t) \approx 0.044t^2$ after the structural transformation (parabola *3* in Fig. 7, *b*). The result of statistical processing of D^* values, measured in the number of movies, is presented as the histogram of the frequencies *f* in Fig. 7, *c*. The curve corresponding to the Gaussian distribution is also provided there. At the reliability level of 0.5, the critical crystal size is $D^* = 0.18 \pm 0.03\ \mu m$.

Figure 8 illustrates the formation of dendrite branches during crystallization of the amorphous HfO_2 film.

On the lateral surface of the first-order single-crystal branch (*1* in Fig. 8, *a*), a small-crystalline interlayer *2* is formed, from which the second-order dendrite branches are formed during the geometric selection of grains growing from this interlayer (*3* in Fig. 8, *a*).

Similarly, on the lateral surface of the second-order single-crystal branches a fine-crystalline layer is formed, from which the third-order dendrite branches will be formed during the geometric selection of grains. And so on. The graph in Fig. 8, *b* illustrates the dependence of

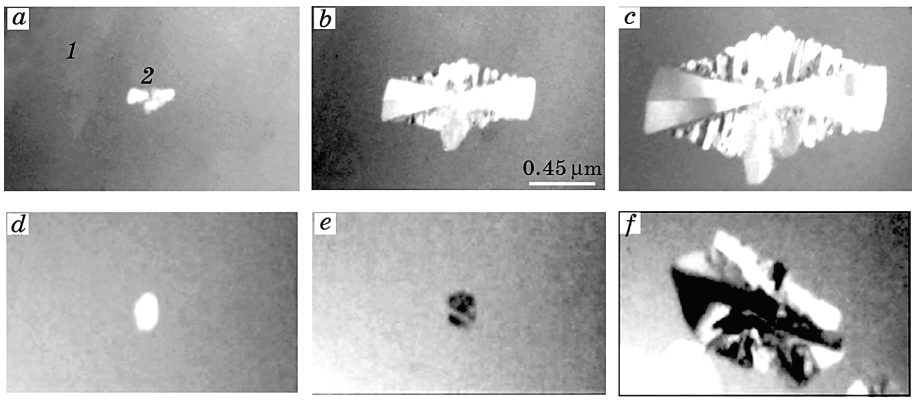

Fig. 6. Dendrite polymorphous crystallization of amorphous film of HfO_2. The single-stage transformation of the amorphous phase—monoclinic modification of HfO_2. The photomicrographs correspond to the periods of time *t*, that passed after the video registration had started: $t = 3.63$ s (*a*), $t = 9.70$ s (*b*), $t = 13.67$ s (*c*). The two-stage transformation of the amorphous phase—the orthorhombic modification of HfO_2–the monoclinic modification of HfO_2. The photomicrographs correspond to the periods of time *t*, that passed after the video registration had started: $t = 2.30$ s (*d*), $t = 2.37$ s (*e*), $t = 4.13$ s (*f*), *1*—amorphous phase, *2*—crystal.

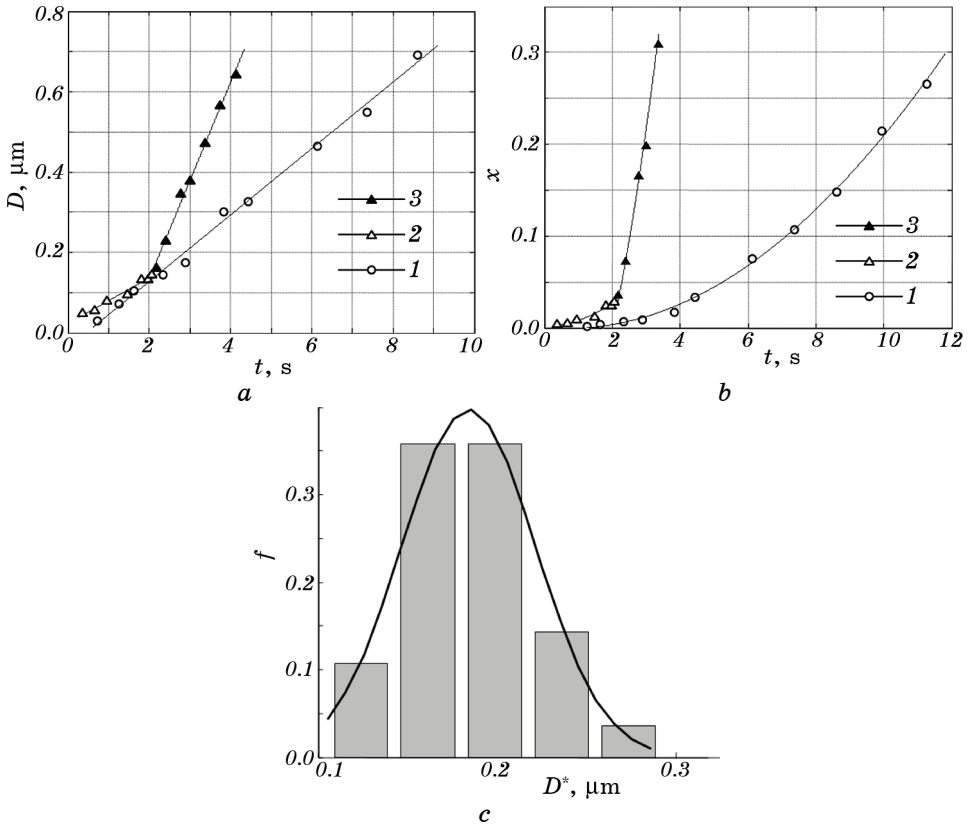

Fig. 7. Kinetics of dendrite polymorphous crystallization of amorphous film of HfO_2. Dependence of the diameter of the dendrite D on time t (*a*). The dependence of the fraction of the crystalline phase x on time t (*b*), *1*—single-stage transformation (amorphous phase–monoclinic modification of HfO_2), *2*—the first part of the two-stage transformation (amorphous phase–orthorhombic modification of HfO_2), *3*—the second part of the two-stage transformation (orthorhombic modification–monoclinic modification of HfO_2). Histogram of the relative frequencies f of the critical diameters D^* of HfO_2 crystals and the curve, which corresponds to the Gaussian distribution (*c*).

the fraction N of 'surviving' crystals on the distance S to the inner boundary of the crystalline interlayer located close to the first-order dendrite branch.

4. CONCLUSION

1. The commonality of crystal growth processes from the vapour phase and from the amorphous state is that in both the cases there is disorder–order transition. This determines the structural and morphologi-

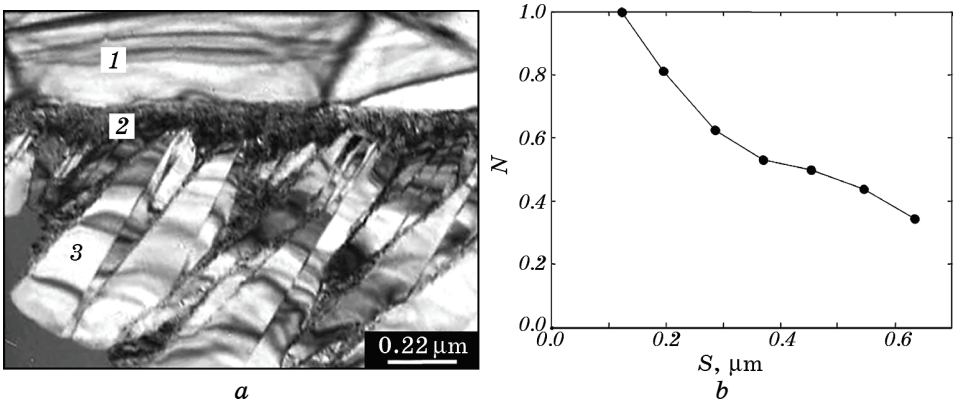

a *b*

Fig. 8. Geometric selection of second-order dendrites branches during polymorphic crystallization of amorphous film of HfO_2 (*a*), *1*—dendrite branch of the first order, *2*—fine-crystalline layer, *3*—second order dendrite branch. Dependence of the fraction N of 'survived' crystals on the distance S to the internal boundary of the fine-crystalline layer.

cal analogy (Table 1) between the main forms of crystal growth on substrates (FM, VW, and SK growth modes) and the main types of crystallization of self-sustained amorphous films (LPC, IPC and DPC).

2. Frank–van der Merwe growth mode corresponds to the type of layer polymorphous crystallization, since in both the cases a single crystal layer is formed. In the case of LPC under the action of the electron beam, the crystals with different morphology (disco-shaped, sickle-shaped and needle-shaped crystals) can be formed in the amorphous film, and each film has its own kinetics of evolution. At the fixed density of the electron beam going through the film, the disk-shaped crystals grow at the constant rate and invariable morphology, for which $x(t) \sim t^2$ and $\delta_0 \sim 2600–4700$. As in the case of the FM growth mode, steps and crystalline layers moving at different speed into the depth of the amorphous matrix may accompany the LPC of amorphous films.

3. Volmer–Weber growth mechanism corresponds to the type of the island polymorphic crystallization, since in both the cases the polycrystalline layer is formed. In the case of LPC of Yb_2O_2S, the average crystal diameter $\langle D \rangle \sim t$, $x(t)$ is described by the exponential relation and $\delta_0 \approx 1000$.

4. The implementation of Stransky–Krastanov growth mode is similar to the type of dendrite polymorphous crystallization, since in both cases the surface of the single-crystal layer serves as the place for the formation of crystals of different orientation. In the case of DPC of HfO_2 single crystals in the form of dendrite branches of the first order are the site of formation of branches of the second and third order. The branches are formed from the series of randomly oriented crystals in

the process of geometric selection.

The author is grateful to the Engineer Nikolai A. Reznik for technical assistance in conducting of the electron microscopic studies and to Maria A. Sokol for the assistance in the design of the article.

REFERENCES

1. U. Köster and U. Herold, *Crystallization of Metallic Glasses* (Eds. H.-J. Güntherodt and H. Beck) (Berlin, Heidelberg: Springer-Verlag: 1981), vol. 46.
2. G.-F. Zhou, *Mater. Sci. Eng. A*, **304–306**: 73 (2001).
3. A. G. Bagmut, *Tech. Phys. Lett.*, **38**: 488 (2012).
4. A. G. Bagmut, *Electronnaya Mikroskopiya Plyonok, Osazhdyonnykh Lazernym Ispareniem* (Kharkiv: NTU 'KhPI': 2014) (in Russian).
5. A. G. Bagmut, *Funct. Mater.*, **26**: 6 (2019).
6. E. Bauer, *Zeitschrift für Kristallographie*, **110**: 372 (1958).
7. E. Bauer and H. Poppa, *Thin Solid Films*, **12**: 167 (1972).
8. D. W. Pashley, M. J. Stowell, M. H. Jacobs, and T. J. Law, *Phil. Mag.*, **10**: 127 (1964).
9. A. G. Bagmut, *Physics of the Solid State*, **59**: 1225 (2017).
10. A. G. Bagmut and I. A. Bagmut, *J. Cryst. Growth*, **517**: 68 (2019).
11. A. Bagmut, *J. Cryst. Growth*, **492**: 92 (2018).
12. A. Bagmut and I. Bagmut, *Mol. Cryst. Liq. Cryst.*, **673**: 120 (2019).
13. S. Le Duc, *Théorie Physico-Chimique de la Vie et Générations Spontanées* (Paris A: Poinat: 1910) (in French).
14. A. G. Bagmut, *J. Synch. Investig.*, **7**: 884 (2013).
15. A. G. Bagmut and A. V. Taran, *J. Adv. Microsc. Res.*, **8**: 57 (2013).
16. G. Ruitenberg, A. K. Petford-Long, and R. C. Doole, *J. Appl. Phys.*, **92**: 3116 (2002).
17. A. G. Bagmut, I. A. Bagmut, V. A. Zhuchkov, and M. O. Shevchenko, *Tech. Phys.*, **57**: 856 (2012).